

Observation of the baryonic B decay $\bar{B}^0 \rightarrow \Lambda_c^+ \bar{K}^-$

J. P. Lees,¹ V. Poireau,¹ V. Tisserand,¹ J. Garra Tico,² E. Grauges,² M. Martinelli^{ab,3} D. A. Milanes^{a,3},
A. Palano^{ab,3} M. Pappagallo^{ab,3} G. Eigen,⁴ B. Stugu,⁴ L. Sun,⁴ D. N. Brown,⁵ L. T. Kerth,⁵ Yu. G. Kolomensky,⁵
G. Lynch,⁵ H. Koch,⁶ T. Schroeder,⁶ D. J. Asgeirsson,⁷ C. Hearty,⁷ T. S. Mattison,⁷ J. A. McKenna,⁷ A. Khan,⁸
V. E. Blinov,⁹ A. R. Buzykaev,⁹ V. P. Druzhinin,⁹ V. B. Golubev,⁹ E. A. Kravchenko,⁹ A. P. Onuchin,⁹
S. I. Serednyakov,⁹ Yu. I. Skovpen,⁹ E. P. Solodov,⁹ K. Yu. Todyshev,⁹ A. N. Yushkov,⁹ M. Bondioli,¹⁰
D. Kirkby,¹⁰ A. J. Lankford,¹⁰ M. Mandelkern,¹⁰ D. P. Stoker,¹⁰ H. Atmacan,¹¹ J. W. Gary,¹¹ F. Liu,¹¹ O. Long,¹¹
G. M. Vitug,¹¹ C. Campagnari,¹² T. M. Hong,¹² D. Kovalskyi,¹² J. D. Richman,¹² C. A. West,¹² A. M. Eisner,¹³
J. Kroseberg,¹³ W. S. Lockman,¹³ A. J. Martinez,¹³ T. Schalk,¹³ B. A. Schumm,¹³ A. Seiden,¹³ C. H. Cheng,¹⁴
D. A. Doll,¹⁴ B. Echenard,¹⁴ K. T. Flood,¹⁴ D. G. Hitlin,¹⁴ P. Ongmongkolkul,¹⁴ F. C. Porter,¹⁴ A. Y. Rakitin,¹⁴
R. Andreassen,¹⁵ M. S. Dubrovin,¹⁵ Z. Huard,¹⁵ B. T. Meadows,¹⁵ M. D. Sokoloff,¹⁵ P. C. Bloom,¹⁶ W. T. Ford,¹⁶
A. Gaz,¹⁶ M. Nagel,¹⁶ U. Nauenberg,¹⁶ J. G. Smith,¹⁶ S. R. Wagner,¹⁶ R. Ayad,^{17,*} W. H. Toki,¹⁷ B. Spaan,¹⁸
M. J. Kobel,¹⁹ K. R. Schubert,¹⁹ R. Schwierz,¹⁹ D. Bernard,²⁰ M. Verderi,²⁰ P. J. Clark,²¹ S. Playfer,²¹
D. Bettoni^{a,22} C. Bozzi^{a,22} R. Calabrese^{ab,22} G. Cibinetto^{ab,22} E. Fioravanti^{ab,22} I. Garzia^{ab,22} E. Luppi^{ab,22}
M. Munerato^{ab,22} M. Negrini^{ab,22} L. Piemontese^{a,22} R. Baldini-Ferroli,²³ A. Calcaterra,²³ R. de Sangro,²³
G. Finocchiaro,²³ M. Nicolaci,²³ P. Patteri,²³ I. M. Peruzzi,^{23,†} M. Piccolo,²³ M. Rama,²³ A. Zallo,²³ R. Contri^{ab,24}
E. Guido^{ab,24} M. Lo Vetere^{ab,24} M. R. Monge^{ab,24} S. Passaggio^{a,24} C. Patrignani^{ab,24} E. Robutti^{a,24} B. Bhuyan,²⁵
V. Prasad,²⁵ C. L. Lee,²⁶ M. Morii,²⁶ A. J. Edwards,²⁷ A. Adametz,²⁸ J. Marks,²⁸ U. Uwer,²⁸ F. U. Bernlochner,²⁹
M. Ebert,²⁹ H. M. Lacker,²⁹ T. Lueck,²⁹ P. D. Dauncey,³⁰ M. Tibbetts,³⁰ P. K. Behera,³¹ U. Mallik,³¹ C. Chen,³²
J. Cochran,³² W. T. Meyer,³² S. Prell,³² E. I. Rosenberg,³² A. E. Rubin,³² A. V. Gritsan,³³ Z. J. Guo,³³
N. Arnaud,³⁴ M. Davier,³⁴ G. Grosdidier,³⁴ F. Le Diberder,³⁴ A. M. Lutz,³⁴ B. Malaescu,³⁴ P. Roudeau,³⁴
M. H. Schune,³⁴ A. Stocchi,³⁴ G. Wormser,³⁴ D. J. Lange,³⁵ D. M. Wright,³⁵ I. Bingham,³⁶ C. A. Chavez,³⁶
J. P. Coleman,³⁶ J. R. Fry,³⁶ E. Gabathuler,³⁶ D. E. Hutchcroft,³⁶ D. J. Payne,³⁶ C. Touramanis,³⁶ A. J. Bevan,³⁷
F. Di Lodovico,³⁷ R. Sacco,³⁷ M. Sigamani,³⁷ G. Cowan,³⁸ S. Paramesvaran,³⁸ D. N. Brown,³⁹ C. L. Davis,³⁹
A. G. Denig,⁴⁰ M. Fritsch,⁴⁰ W. Gradl,⁴⁰ A. Hafner,⁴⁰ E. Prencipe,⁴⁰ K. E. Alwyn,⁴¹ D. Bailey,⁴¹ R. J. Barlow,^{41,‡}
G. Jackson,⁴¹ G. D. Lafferty,⁴¹ R. Cenci,⁴² B. Hamilton,⁴² A. Jawahery,⁴² D. A. Roberts,⁴² G. Simi,⁴²
C. Dallapiccola,⁴³ R. Cowan,⁴⁴ D. Dujmic,⁴⁴ G. Sciolla,⁴⁴ D. Lindemann,⁴⁵ P. M. Patel,⁴⁵ S. H. Robertson,⁴⁵
M. Schram,⁴⁵ P. Biassoni^{ab,46} A. Lazzaro^{ab,46} V. Lombardo^{a,46} N. Neri^{ab,46} F. Palombo^{ab,46} S. Stracka^{ab,46}
L. Cremaldi,⁴⁷ R. Godang,^{47,§} R. Kroeger,⁴⁷ P. Sonnek,⁴⁷ D. J. Summers,⁴⁷ X. Nguyen,⁴⁸ P. Taras,⁴⁸ G. De
Nardo^{ab,49} D. Monorchio^{ab,49} G. Onorato^{ab,49} C. Sciacca^{ab,49} G. Raven,⁵⁰ H. L. Snoek,⁵⁰ C. P. Jessop,⁵¹
K. J. Knoepfel,⁵¹ J. M. LoSecco,⁵¹ W. F. Wang,⁵¹ K. Honscheid,⁵² R. Kass,⁵² J. Brau,⁵³ R. Frey,⁵³ N. B. Sinev,⁵³
D. Strom,⁵³ E. Torrence,⁵³ E. Feltresi^{ab,54} N. Gagliardi^{ab,54} M. Margoni^{ab,54} M. Morandin^{a,54} M. Posocco^{a,54}
M. Rotondo^{a,54} F. Simonetto^{ab,54} R. Stroili^{ab,54} E. Ben-Haim,⁵⁵ M. Bomben,⁵⁵ G. R. Bonneaud,⁵⁵ H. Briand,⁵⁵
G. Calderini,⁵⁵ J. Chauveau,⁵⁵ O. Hamon,⁵⁵ Ph. Leruste,⁵⁵ G. Marchiori,⁵⁵ J. Ocariz,⁵⁵ S. Sitt,⁵⁵ M. Biasini^{ab,56}
E. Manoni^{ab,56} S. Pacetti^{ab,56} A. Rossi^{ab,56} C. Angelini^{ab,57} G. Batignani^{ab,57} S. Bettarini^{ab,57} M. Carpinelli^{ab,57,¶}
G. Casarosa^{ab,57} A. Cervelli^{ab,57} F. Forti^{ab,57} M. A. Giorgi^{ab,57} A. Lusiani^{ac,57} B. Oberhof^{ab,57} E. Paoloni^{ab,57}
A. Perez^{a,57} G. Rizzo^{ab,57} J. J. Walsh^{a,57} D. Lopes Pegna,⁵⁸ C. Lu,⁵⁸ J. Olsen,⁵⁸ A. J. S. Smith,⁵⁸
A. V. Telnov,⁵⁸ F. Anulli^{a,59} G. Cavoto^{a,59} R. Faccini^{ab,59} F. Ferrarotto^{a,59} F. Ferroni^{ab,59} M. Gaspero^{ab,59}
L. Li Gioi^{a,59} M. A. Mazzoni^{a,59} G. Piredda^{a,59} C. Büniger,⁶⁰ O. Grünberg,⁶⁰ T. Hartmann,⁶⁰ T. Leddig,⁶⁰
H. Schröder,⁶⁰ R. Waldi,⁶⁰ T. Adye,⁶¹ E. O. Olaiya,⁶¹ F. F. Wilson,⁶¹ S. Emery,⁶² G. Hamel de Monchenault,⁶²
G. Vasseur,⁶² Ch. Yèche,⁶² D. Aston,⁶³ D. J. Bard,⁶³ R. Bartoldus,⁶³ C. Cartaro,⁶³ M. R. Convery,⁶³
J. Dorfan,⁶³ G. P. Dubois-Felsmann,⁶³ W. Dunwoodie,⁶³ R. C. Field,⁶³ M. Franco Sevilla,⁶³ B. G. Fulsom,⁶³
A. M. Gabareen,⁶³ M. T. Graham,⁶³ P. Grenier,⁶³ C. Hast,⁶³ W. R. Innes,⁶³ M. H. Kelsey,⁶³ H. Kim,⁶³ P. Kim,⁶³
M. L. Kocian,⁶³ D. W. G. S. Leith,⁶³ P. Lewis,⁶³ S. Li,⁶³ B. Lindquist,⁶³ S. Luitz,⁶³ V. Luth,⁶³ H. L. Lynch,⁶³
D. B. MacFarlane,⁶³ D. R. Muller,⁶³ H. Neal,⁶³ S. Nelson,⁶³ I. Ofte,⁶³ M. Perl,⁶³ T. Pulliam,⁶³ B. N. Ratcliff,⁶³
A. Roodman,⁶³ A. A. Salnikov,⁶³ V. Santoro,⁶³ R. H. Schindler,⁶³ A. Snyder,⁶³ D. Su,⁶³ M. K. Sullivan,⁶³
J. Va'vra,⁶³ A. P. Wagner,⁶³ M. Weaver,⁶³ W. J. Wisniewski,⁶³ M. Wittgen,⁶³ D. H. Wright,⁶³ H. W. Wulsin,⁶³

A. K. Yarritu,⁶³ C. C. Young,⁶³ V. Ziegler,⁶³ W. Park,⁶⁴ M. V. Purohit,⁶⁴ R. M. White,⁶⁴ J. R. Wilson,⁶⁴
 A. Randle-Conde,⁶⁵ S. J. Sekula,⁶⁵ M. Bellis,⁶⁶ J. F. Benitez,⁶⁶ P. R. Burchat,⁶⁶ T. S. Miyashita,⁶⁶ M. S. Alam,⁶⁷
 J. A. Ernst,⁶⁷ R. Gorodeisky,⁶⁸ N. Guttman,⁶⁸ D. R. Peimer,⁶⁸ A. Soffer,⁶⁸ P. Lund,⁶⁹ S. M. Spanier,⁶⁹
 R. Eckmann,⁷⁰ J. L. Ritchie,⁷⁰ A. M. Ruland,⁷⁰ C. J. Schilling,⁷⁰ R. F. Schwitters,⁷⁰ B. C. Wray,⁷⁰ J. M. Izen,⁷¹
 X. C. Lou,⁷¹ F. Bianchi^{ab,72} D. Gamba^{ab,72} L. Lanceri^{ab,73} L. Vitale^{ab,73} F. Martinez-Vidal,⁷⁴ A. Oyanguren,⁷⁴
 H. Ahmed,⁷⁵ J. Albert,⁷⁵ Sw. Banerjee,⁷⁵ H. H. F. Choi,⁷⁵ G. J. King,⁷⁵ R. Kowalewski,⁷⁵ M. J. Lewczuk,⁷⁵
 C. Lindsay,⁷⁵ I. M. Nugent,⁷⁵ J. M. Roney,⁷⁵ R. J. Sobie,⁷⁵ T. J. Gershon,⁷⁶ P. F. Harrison,⁷⁶ T. E. Latham,⁷⁶
 E. M. T. Puccio,⁷⁶ H. R. Band,⁷⁷ S. Dasu,⁷⁷ Y. Pan,⁷⁷ R. Prepost,⁷⁷ C. O. Vuosalo,⁷⁷ and S. L. Wu⁷⁷

(The BABAR Collaboration)

¹Laboratoire d'Annecy-le-Vieux de Physique des Particules (LAPP),
 Université de Savoie, CNRS/IN2P3, F-74941 Annecy-Le-Vieux, France

²Universitat de Barcelona, Facultat de Física, Departament ECM, E-08028 Barcelona, Spain

³INFN Sezione di Bari^a; Dipartimento di Fisica, Università di Bari^b, I-70126 Bari, Italy

⁴University of Bergen, Institute of Physics, N-5007 Bergen, Norway

⁵Lawrence Berkeley National Laboratory and University of California, Berkeley, California 94720, USA

⁶Ruhr Universität Bochum, Institut für Experimentalphysik 1, D-44780 Bochum, Germany

⁷University of British Columbia, Vancouver, British Columbia, Canada V6T 1Z1

⁸Brunel University, Uxbridge, Middlesex UB8 3PH, United Kingdom

⁹Budker Institute of Nuclear Physics, Novosibirsk 630090, Russia

¹⁰University of California at Irvine, Irvine, California 92697, USA

¹¹University of California at Riverside, Riverside, California 92521, USA

¹²University of California at Santa Barbara, Santa Barbara, California 93106, USA

¹³University of California at Santa Cruz, Institute for Particle Physics, Santa Cruz, California 95064, USA

¹⁴California Institute of Technology, Pasadena, California 91125, USA

¹⁵University of Cincinnati, Cincinnati, Ohio 45221, USA

¹⁶University of Colorado, Boulder, Colorado 80309, USA

¹⁷Colorado State University, Fort Collins, Colorado 80523, USA

¹⁸Technische Universität Dortmund, Fakultät Physik, D-44221 Dortmund, Germany

¹⁹Technische Universität Dresden, Institut für Kern- und Teilchenphysik, D-01062 Dresden, Germany

²⁰Laboratoire Leprince-Ringuet, Ecole Polytechnique, CNRS/IN2P3, F-91128 Palaiseau, France

²¹University of Edinburgh, Edinburgh EH9 3JZ, United Kingdom

²²INFN Sezione di Ferrara^a; Dipartimento di Fisica, Università di Ferrara^b, I-44100 Ferrara, Italy

²³INFN Laboratori Nazionali di Frascati, I-00044 Frascati, Italy

²⁴INFN Sezione di Genova^a; Dipartimento di Fisica, Università di Genova^b, I-16146 Genova, Italy

²⁵Indian Institute of Technology Guwahati, Guwahati, Assam, 781 039, India

²⁶Harvard University, Cambridge, Massachusetts 02138, USA

²⁷Harvey Mudd College, Claremont, California 91711

²⁸Universität Heidelberg, Physikalisches Institut, Philosophenweg 12, D-69120 Heidelberg, Germany

²⁹Humboldt-Universität zu Berlin, Institut für Physik, Newtonstr. 15, D-12489 Berlin, Germany

³⁰Imperial College London, London, SW7 2AZ, United Kingdom

³¹University of Iowa, Iowa City, Iowa 52242, USA

³²Iowa State University, Ames, Iowa 50011-3160, USA

³³Johns Hopkins University, Baltimore, Maryland 21218, USA

³⁴Laboratoire de l'Accélérateur Linéaire, IN2P3/CNRS et Université Paris-Sud 11,
 Centre Scientifique d'Orsay, B. P. 34, F-91898 Orsay Cedex, France

³⁵Lawrence Livermore National Laboratory, Livermore, California 94550, USA

³⁶University of Liverpool, Liverpool L69 7ZE, United Kingdom

³⁷Queen Mary, University of London, London, E1 4NS, United Kingdom

³⁸University of London, Royal Holloway and Bedford New College, Egham, Surrey TW20 0EX, United Kingdom

³⁹University of Louisville, Louisville, Kentucky 40292, USA

⁴⁰Johannes Gutenberg-Universität Mainz, Institut für Kernphysik, D-55099 Mainz, Germany

⁴¹University of Manchester, Manchester M13 9PL, United Kingdom

⁴²University of Maryland, College Park, Maryland 20742, USA

⁴³University of Massachusetts, Amherst, Massachusetts 01003, USA

⁴⁴Massachusetts Institute of Technology, Laboratory for Nuclear Science, Cambridge, Massachusetts 02139, USA

⁴⁵McGill University, Montréal, Québec, Canada H3A 2T8

⁴⁶INFN Sezione di Milano^a; Dipartimento di Fisica, Università di Milano^b, I-20133 Milano, Italy

⁴⁷University of Mississippi, University, Mississippi 38677, USA

⁴⁸Université de Montréal, Physique des Particules, Montréal, Québec, Canada H3C 3J7

⁴⁹INFN Sezione di Napoli^a; Dipartimento di Scienze Fisiche,
 Università di Napoli Federico II^b, I-80126 Napoli, Italy

⁵⁰NIKHEF, National Institute for Nuclear Physics and High Energy Physics, NL-1009 DB Amsterdam, The Netherlands

⁵¹University of Notre Dame, Notre Dame, Indiana 46556, USA

⁵²Ohio State University, Columbus, Ohio 43210, USA

⁵³University of Oregon, Eugene, Oregon 97403, USA

⁵⁴INFN Sezione di Padova^a; Dipartimento di Fisica, Università di Padova^b, I-35131 Padova, Italy

⁵⁵Laboratoire de Physique Nucléaire et de Hautes Energies,

IN2P3/CNRS, Université Pierre et Marie Curie-Paris6,

Université Denis Diderot-Paris7, F-75252 Paris, France

⁵⁶INFN Sezione di Perugia^a; Dipartimento di Fisica, Università di Perugia^b, I-06100 Perugia, Italy

⁵⁷INFN Sezione di Pisa^a; Dipartimento di Fisica,

Università di Pisa^b; Scuola Normale Superiore di Pisa^c, I-56127 Pisa, Italy

⁵⁸Princeton University, Princeton, New Jersey 08544, USA

⁵⁹INFN Sezione di Roma^a; Dipartimento di Fisica,

Università di Roma La Sapienza^b, I-00185 Roma, Italy

⁶⁰Universität Rostock, D-18051 Rostock, Germany

⁶¹Rutherford Appleton Laboratory, Chilton, Didcot, Oxon, OX11 0QX, United Kingdom

⁶²CEA, Irfu, SPP, Centre de Saclay, F-91191 Gif-sur-Yvette, France

⁶³SLAC National Accelerator Laboratory, Stanford, California 94309 USA

⁶⁴University of South Carolina, Columbia, South Carolina 29208, USA

⁶⁵Southern Methodist University, Dallas, Texas 75275, USA

⁶⁶Stanford University, Stanford, California 94305-4060, USA

⁶⁷State University of New York, Albany, New York 12222, USA

⁶⁸Tel Aviv University, School of Physics and Astronomy, Tel Aviv, 69978, Israel

⁶⁹University of Tennessee, Knoxville, Tennessee 37996, USA

⁷⁰University of Texas at Austin, Austin, Texas 78712, USA

⁷¹University of Texas at Dallas, Richardson, Texas 75083, USA

⁷²INFN Sezione di Torino^a; Dipartimento di Fisica Sperimentale, Università di Torino^b, I-10125 Torino, Italy

⁷³INFN Sezione di Trieste^a; Dipartimento di Fisica, Università di Trieste^b, I-34127 Trieste, Italy

⁷⁴IFIC, Universitat de Valencia-CSIC, E-46071 Valencia, Spain

⁷⁵University of Victoria, Victoria, British Columbia, Canada V8W 3P6

⁷⁶Department of Physics, University of Warwick, Coventry CV4 7AL, United Kingdom

⁷⁷University of Wisconsin, Madison, Wisconsin 53706, USA

(Dated: August 16, 2011)

We report the observation of the baryonic B decay $\bar{B}^0 \rightarrow \Lambda_c^+ \bar{\Lambda} K^-$ with a significance larger than 7 standard deviations based on $471 \times 10^6 B\bar{B}$ pairs collected with the BABAR detector at the PEP-II storage ring at SLAC. We measure the branching fraction for the decay $\bar{B}^0 \rightarrow \Lambda_c^+ \bar{\Lambda} K^-$ to be $(3.8 \pm 0.8_{\text{stat}} \pm 0.2_{\text{sys}} \pm 1.0_{\Lambda_c^+}) \times 10^{-5}$. The uncertainties are statistical, systematic, and due to the uncertainty in the Λ_c^+ branching fraction. We find that the $\Lambda_c^+ K^-$ invariant mass distribution shows an enhancement above $3.5 \text{ GeV}/c^2$.

PACS numbers: 13.25.Hw, 13.60.Rj, 14.20.Lq

While baryons are produced in $(6.8 \pm 0.6)\%$ [1] of all B -meson decays, little is known about the detailed mechanics of these decays and more generally about hadron fragmentation into baryons. We can increase our understanding of baryon production in B decays by comparing decay rates for related exclusive final states. In this paper we present a measurement of the decay $\bar{B}^0 \rightarrow \Lambda_c^+ \bar{\Lambda} K^-$ [2]. Currently, no experimental results are available for this decay.

This analysis is based on a dataset of about 429 fb^{-1} , corresponding to $471 \times 10^6 B\bar{B}$ pairs, collected with the BABAR detector at the PEP-II asymmetric-energy e^+e^- storage ring, operated at a center-of-mass energy equal to the $\Upsilon(4S)$ mass. The signal efficiency is determined with a Monte Carlo simulation based on EvtGen [3] for the event generation, and GEANT4 [4] for the detector simulation. The $\bar{B}^0 \rightarrow \Lambda_c^+ \bar{\Lambda} K^-$ Monte Carlo events are

generated uniformly in the $\Lambda_c^+ \bar{\Lambda} K^-$ phase space. Monte Carlo simulated events are used to study background contributions as well.

The BABAR detector is described in detail elsewhere [5]. Charged particle trajectories are measured by a five-layer double-sided silicon vertex tracker and a 40-layer drift chamber, both immersed in a 1.5 T axial magnetic field. Charged particle identification is provided by ionization energy measurements along with Cherenkov radiation detection by an internally reflecting ring-imaging detector (DIRC).

The Λ_c^+ is reconstructed in the decay mode $\Lambda_c^+ \rightarrow pK^-\pi^+$ and the $\bar{\Lambda}$ in the decay mode $\bar{\Lambda} \rightarrow \bar{p}\pi^+$. For the identification of proton, kaon, and pion candidates, we use selection criteria based on the measurements of the specific ionization in the tracking detectors, and of the Cherenkov radiation in the DIRC [6].

For the identification of the p coming from the Λ_c^+ the average efficiency is about 95% while the probability of misidentifying a kaon as a proton is less than 2%. The average efficiency for the K^- identification is about 90%. The probability of misidentifying a pion as a kaon is about 5%. These are the dominant misidentification probabilities for each particle type. The Λ_c^+ daughters and the $\bar{\Lambda}$ daughters are each fit to a common vertex and the Λ_c^+ and the $\bar{\Lambda}$ candidate invariant mass is required to lie within 3σ of the world average mass[1]; i.e., in the range 2.273 to 2.299 GeV/ c^2 and 1.113 to 1.119 GeV/ c^2 , respectively. For the reconstruction of the B candidate, the mass of the Λ_c^+ candidate is constrained to its nominal value [1] and is combined with a $\bar{\Lambda}$ and a K^- candidate. Since the $\bar{\Lambda}$ candidate mass is already well measured, it is not constrained.

The Λ_c^+ , $\bar{\Lambda}$ and K^- candidates are then fitted to a common vertex and the confidence level of this fit is required to exceed 0.2%.

A possible source for fake signal events is the decay $\bar{B}^0 \rightarrow \Lambda_c^+ \bar{p} K^- \pi^+$ [7], which has the same final state as the decay under investigation. In order to suppress this background we require that the distance between the B vertex and the $\bar{\Lambda}$ vertex in the xy plane (with z parallel to the beam axis) exceeds 0.4 cm. This constraint reduces combinatoric background by 18%, and the background from $\bar{B}^0 \rightarrow \Lambda_c^+ \bar{p} K^- \pi^+$ by 99.6%. The expected remaining background from this decay is determined to be 0.1 ± 0.1 events[7].

The separation of signal and background in the candidate sample is obtained by using two kinematic variables, $\Delta E = E_B^* - \sqrt{s}/2$ and $m_{ES} = \sqrt{(s/2 + \mathbf{p}_i \cdot \mathbf{p}_B)^2/E_i^2 - |\mathbf{p}_B|^2}$, where \sqrt{s} is the e^+e^- center-of-mass energy and E_B^* the energy of the B candidate in the center-of-mass system. (E_i, \mathbf{p}_i) is the four-momentum vector of the e^+e^- system and \mathbf{p}_B the B -candidate momentum vector, both measured in the laboratory frame. For true B decays m_{ES} is centered at the B -meson mass and ΔE is centered at zero. B candidates are required to have an m_{ES} value between 5.272 and 5.288 GeV/ c^2 .

Figure 1 shows the ΔE distribution of the selected candidates, fitted in the range from -0.12 to 0.30 GeV. We fit the signal with a Gaussian with the mean μ and width σ fixed to the values obtained from a fit to the Monte Carlo simulation ($\mu = 0.247$ MeV and $\sigma = 8.381$ MeV), leaving only the signal yield floating. The background is described by a first-order polynomial. A binned maximum likelihood fit with this probability density function (PDF) gives a signal yield of 51 ± 9 events. (For the branching fraction measurement described later, we use the excess number of candidates above background as the estimate of the number of signal events.) The confidence level for the null hypothesis, considering statistical uncertainties only, is 2.6×10^{-15} , which corresponds

to a statistical significance of 8 standard deviations. A possible background from $\bar{B}^0 \rightarrow \Lambda_c^+ \Sigma^0 K^-$, which rises slowly up to $\Delta E \approx -0.06$ GeV and drops sharply between $\Delta E = -0.05$ GeV and -0.02 GeV, is not visible in Fig. 1.

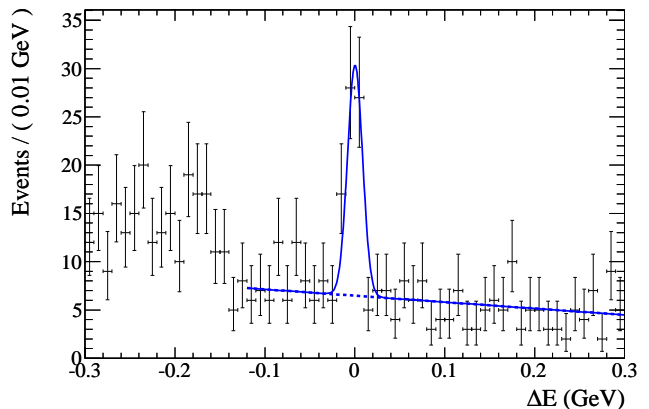


FIG. 1: The ΔE distribution for $\Lambda_c^+ \bar{\Lambda} K^-$ candidates in data with all selection criteria applied (points). The solid line is the overall fit result, while the dashed line is the background component.

Since the decay dynamics of baryonic B decays are largely unknown, we investigate the invariant-mass distribution of the two-body systems. Intermediate states would appear as differences in the invariant-mass distribution for data and for the $\bar{B}^0 \rightarrow \Lambda_c^+ \bar{\Lambda} K^-$ Monte Carlo simulation, in which the final state is generated according to three-body phase space. Using the same function that we used in Fig. 1, we fit the ΔE distributions for ten ranges of the three two-body masses. The results are compared to the phase space Monte Carlo simulation in Fig. 2. While the $m(\Lambda_c^+ \bar{\Lambda})$ and $m(\bar{\Lambda} K^-)$ distributions show no significant deviations, the $m(\Lambda_c^+ K^-)$ distribution shows the data concentrated in the upper half of the allowed mass range, contrary to the Monte Carlo simulation. A possible explanation for this is a resonant decay via a baryon resonance that has not yet been observed. Another possibility is enhanced rates at both $m(\Lambda_c^+ \bar{\Lambda})$ and $m(\bar{\Lambda} K^-)$ thresholds.

Because the efficiency varies over the Dalitz plot and the distribution of candidates in data is unknown *a priori*, we must use the distribution of the data events in the Dalitz plot to estimate the efficiency. The small number of candidates, combined with resolution and edge effects, make the simple weighting of events by the inverse of the efficiency problematic. Instead we determine a set of weights to apply to the simulated events so that the resulting weighted Monte Carlo distributions mimic the data. We make the assumption that the dependence of the decay dynamics on the two-body invariant masses can be factorized into the product of three functions that each depend on one invariant mass and weight the Monte

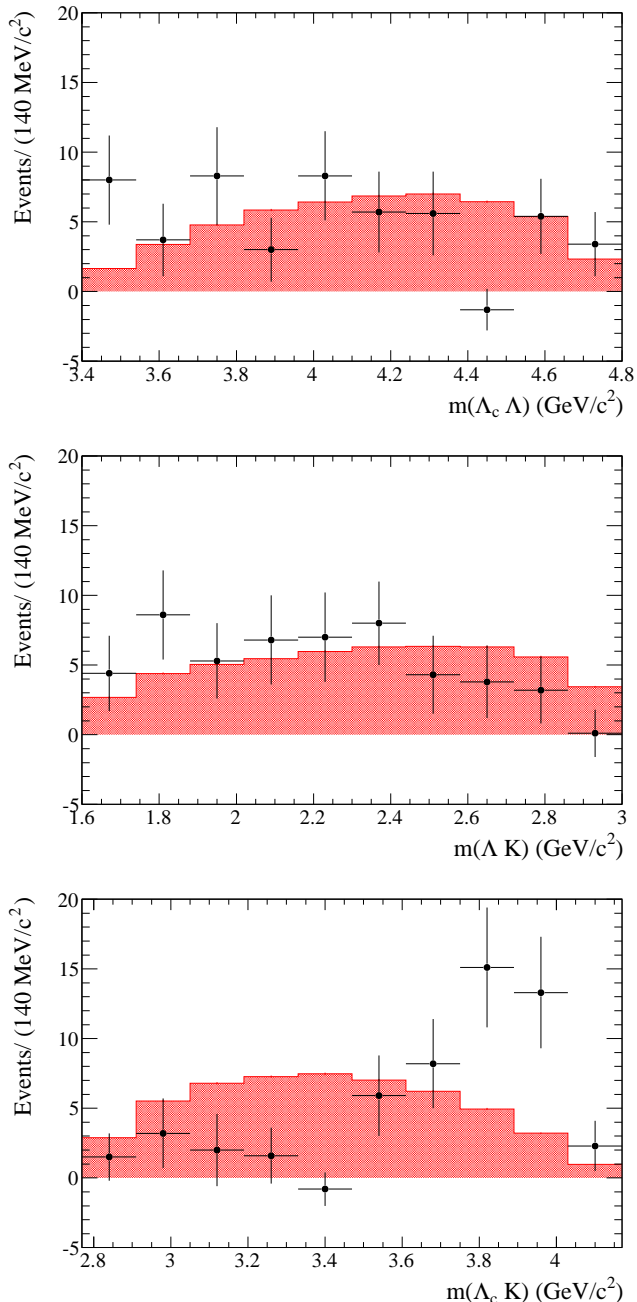


FIG. 2: The $m(\Lambda_c^+ \bar{\Lambda})$, $m(\bar{\Lambda} K^-)$ and $m(\Lambda_c^+ K^-)$ distributions in data (points) in comparison with the Monte Carlo sample (red histogram).

Carlo events with the function:

$$\begin{aligned}
 & w[m(\Lambda_c^+ K^-), m(\Lambda_c^+ \bar{\Lambda}), m(\bar{\Lambda} K^-)] \\
 & = w_a[m(\Lambda_c^+ K^-)] \cdot w_b[m(\Lambda_c^+ \bar{\Lambda})] \cdot w_c[m(\bar{\Lambda} K^-)]. \quad (1)
 \end{aligned}$$

By dividing the background subtracted $m(\Lambda_c^+ K^-)$ distribution (Fig. 2) by the corresponding distribution from the phase-space Monte Carlo simulation, we obtain the weights $w_a[m(\Lambda_c^+ K^-)]$, which are used to weight

TABLE I: Two-body invariant mass distributions used for the weighting and the corresponding reconstruction efficiency ε . The dots indicate how often the respective mass distributions are used to determine the weights.

$m(\Lambda_c^+ K^-)$	$m(\Lambda_c^+ \bar{\Lambda})$	$m(\bar{\Lambda} K^-)$	Efficiency ε in %
			10.90
•			8.60
•	•		9.21
•	•	•	9.19
••	•	•	8.81
••	••	•	8.80
••	••	••	8.77

the Monte Carlo candidates. (If a negative weight is required the weight is constrained to zero.) Next, we use the weighted Monte Carlo candidates to determine $w_b[m(\Lambda_c^+ \bar{\Lambda})]$ in the same way and then use $w_a[m(\Lambda_c^+ K^-)] \cdot w_b[m(\Lambda_c^+ \bar{\Lambda})]$ to determine $w_c[m(\bar{\Lambda} K^-)]$. After each weighting we determine the reconstruction efficiency by a fit to the ΔE distribution for weighted Monte Carlo. Starting with these weights, the weighting is repeated until the reconstruction efficiency converges and the two-body mass distributions in data and Monte Carlo agree within statistical uncertainties. The efficiency after each weighting is shown in Table I. Since the $m(\Lambda_c^+ K^-)$ distribution in data shows the strongest deviations compared to the phase space Monte Carlo simulation we use the efficiency ε obtained after the second weighting in $m(\Lambda_c^+ K^-)$ [$\varepsilon = 8.81\%$]. The comparison between data and weighted Monte Carlo events in the two-body masses can be seen in Fig. 3. Note that, by construction, the data and simulation agree exactly for the $m(\Lambda_c^+ K^-)$ distribution. The close agreement in the other two distributions shows that the form given in Eq. (1) is adequate to describe any correlations between variables in the data. The effect of the statistical uncertainties in the data on the efficiency determination is described below.

For the branching fraction calculation we determine the number of reconstructed events by a fit to ΔE with a first-order polynomial for the background. To avoid a potential bias introduced by an assumption of the signal shape, we fit the region $-0.12 < \Delta E < 0.30$ GeV exclusive of the signal region $-0.03 < \Delta E < 0.03$ GeV. By extrapolating the background yield into the signal region and subtracting it from the integral of the histogram in this region we obtain a signal yield of $N_{\text{sig}} = 50 \pm 11$. This results in a branching fraction of

$$\begin{aligned}
 & \mathcal{B}(\bar{B}^0 \rightarrow \Lambda_c^+ \bar{\Lambda} K^-) \\
 & = \frac{N_{\text{sig}}/\varepsilon}{N_{B\bar{B}} \cdot \mathcal{B}(\Lambda_c^+ \rightarrow p K^- \pi^+) \cdot \mathcal{B}(\bar{\Lambda} \rightarrow \bar{p} \pi^+)} \\
 & = (3.8 \pm 0.8_{\text{stat}} \pm 1.0_{\Lambda_c^+}) \times 10^{-5}, \quad (2)
 \end{aligned}$$

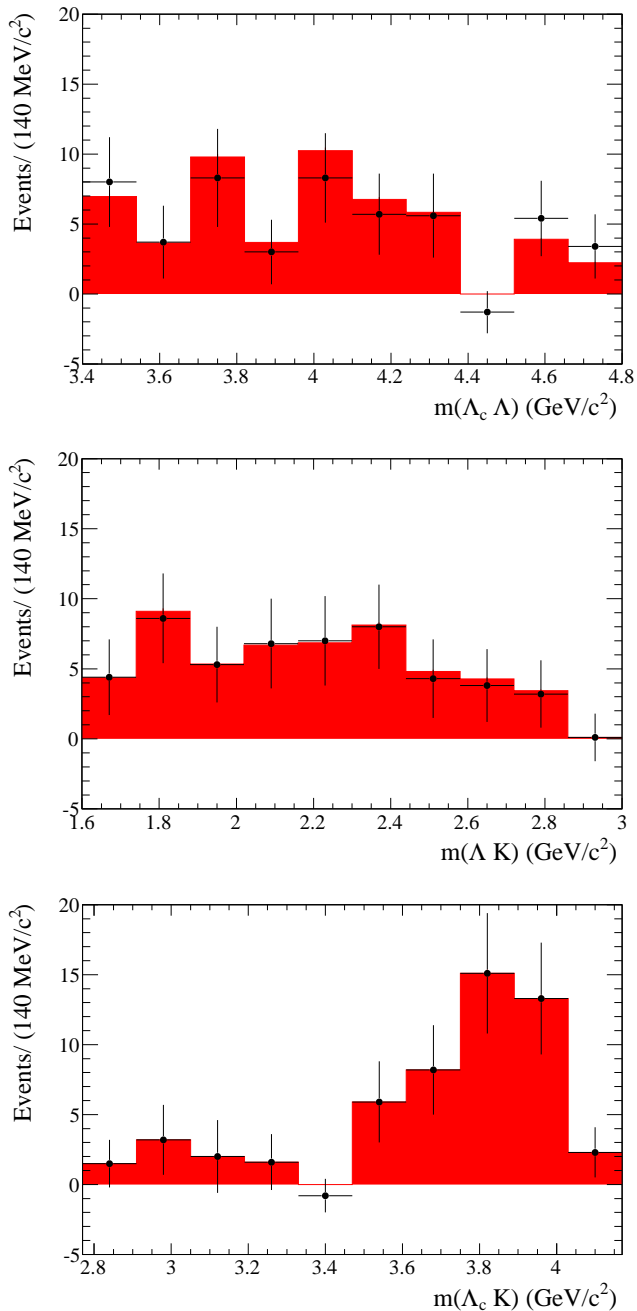


FIG. 3: The background-subtracted $m(\Lambda_c^+ \bar{\Lambda})$, $m(\bar{\Lambda} K^-)$ and $m(\Lambda_c^+ K^-)$ distributions for data (points) and for the final weighted Monte Carlo sample (red histogram).

with $N_{B\bar{B}} = N_{\bar{B}^0} + N_{B^0} = (471 \pm 3) \times 10^6$, assuming equal production of $\bar{B}^0 \bar{B}^0$ and $B^+ B^-$ in the decay of the $\Upsilon(4S)$. The branching fractions $\mathcal{B}(\Lambda_c^+ \rightarrow p K^- \pi^+) = (5.0 \pm 1.3)\%$ and $\mathcal{B}(\bar{\Lambda} \rightarrow \bar{p} \pi^+) = (63.9 \pm 0.5)\%$ are the world averages from Ref. [1].

Several sources of systematic uncertainties are investigated and summarized in Table II. Most of the uncertainties are derived from comparisons between Monte

Carlo simulations and control samples in data. Systematic uncertainties arise from uncertainties in charged particle reconstruction efficiencies (0.9%) and charged particle identification efficiencies (2.4%), and from statistical uncertainties in the Monte Carlo simulation (0.5%). The systematic uncertainty on the number of $B\bar{B}$ pairs is 0.6%. The systematic uncertainty from the $\bar{\Lambda}$ branching fraction amounts to 0.8%.

The systematic uncertainty introduced by neglecting a possible $\bar{B}^0 \rightarrow \Lambda_c^+ \bar{\Sigma}^0 K^-$ background is determined by adding a PDF for this background to the fit function used for the ΔE fit shown in Fig. 1. Allowing nonnegative contributions from this background, the fit returns a value of $0.0_{-0.0}^{+1.8}$. For a conservative limit on this systematic uncertainty we fix the yield to 1.8 and take the change in the number of signal events as systematic uncertainty (1.0%). The ΔE distribution in Fig. 1 shows an enhancement below -0.14 GeV, caused by decays of the type $B \rightarrow \Lambda_c^+ \bar{\Lambda} K^- \pi$. Due to the limited resolution these events could leak into the fit region from -0.12 to 0.30 GeV. We determine the resulting systematic uncertainty by changing the fit region to -0.10 to 0.30 GeV. The branching fraction changes by 1.8%.

The uncertainty arising from the chosen background description is determined by repeating the fit to determine the signal yield with a second-order polynomial for the background. The number of signal events changes by 2.0%. A comparison between data and Monte Carlo events shows that the mean of the ΔE distribution in data is shifted by -0.003 GeV. We determine the resulting systematic uncertainty by shifting the signal region for the fit in the Monte Carlo ΔE distribution by 0.003 GeV. This changes the efficiency to 8.60%, corresponding to a systematic uncertainty of 0.8%.

The uncertainty due to the treatment of the three-body phase space in the efficiency correction is estimated from the variation of the efficiency when performing further iterations of weighting. Table I shows a variation from 8.81% down to 8.77%. This corresponds to a systematic uncertainty of 0.5%.

A possible additional contribution to the statistical uncertainty coming from the efficiency determination, where we determined the weights based on data events in ranges of the two-body masses, is studied by performing the efficiency correction in ranges of $m(\Lambda_c^+ K^-)$ only, with unweighted Monte Carlo events. The change in overall reconstruction efficiency is negligible compared to the statistical uncertainty.

Adding all contributions in quadrature we obtain a systematic uncertainty of 4.1%. The significance of the signal, including additive systematic uncertainties is determined to be more than 7 standard deviations. This significance includes systematic uncertainties from the $\bar{B}^0 \rightarrow \Lambda_c^+ \bar{\Sigma}^0 K^-$ and $B \rightarrow \Lambda_c^+ \bar{\Lambda} K^- \pi$ background as well as the ΔE background description.

In summary, we observe the decay $\bar{B}^0 \rightarrow \Lambda_c^+ \bar{\Lambda} K^-$ with

TABLE II: Summary of the relative systematic uncertainties on the branching fraction $\mathcal{B}(\bar{B}^0 \rightarrow \Lambda_c^+ \bar{\Lambda} K^-)$.

Source	Relative syst. uncert.
Track reconstruction	0.9%
Charged particle ID	2.4%
$N_{B\bar{B}}$	0.6%
$\mathcal{B}(\bar{\Lambda} \rightarrow \bar{p}\pi^+)$	0.8%
Monte Carlo statistics	0.5%
$\bar{B}^0 \rightarrow \Lambda_c^+ \bar{\Sigma}^0 K^-$	1.0%
$B \rightarrow \Lambda_c^+ \bar{\Lambda} K^- \pi$	1.8%
ΔE background description	2.0%
$\mu(\Delta E)$ shift	0.8%
Efficiency determination	0.5%
Total	4.1%

a significance larger than 7 standard deviations and measure a branching fraction of

$$\begin{aligned} \mathcal{B}(\bar{B}^0 \rightarrow \Lambda_c^+ \bar{\Lambda} K^-) \\ = (3.8 \pm 0.8_{\text{stat}} \pm 0.2_{\text{sys}} \pm 1.0_{\Lambda_c^+}) \times 10^{-5}. \end{aligned} \quad (3)$$

The decay rate is not uniform over three-body phase space; rather, it is dominant at high $\Lambda_c^+ K^-$ mass.

We are grateful for the excellent luminosity and machine conditions provided by our PEP-II colleagues, and for the substantial dedicated effort from the computing organizations that support *BABAR*. The collaborating institutions wish to thank SLAC for its support and kind hospitality. This work is supported by DOE and NSF (USA), NSERC (Canada), CEA and CNRS-IN2P3

(France), BMBF and DFG (Germany), INFN (Italy), FOM (The Netherlands), NFR (Norway), MES (Russia), MICIIN (Spain), STFC (United Kingdom). Individuals have received support from the Marie Curie EIF (European Union), the A. P. Sloan Foundation (USA) and the Binational Science Foundation (USA-Israel).

* Now at Temple University, Philadelphia, Pennsylvania 19122, USA

† Also with Università di Perugia, Dipartimento di Fisica, Perugia, Italy

‡ Now at the University of Huddersfield, Huddersfield HD1 3DH, UK

§ Now at University of South Alabama, Mobile, Alabama 36688, USA

¶ Also with Università di Sassari, Sassari, Italy

- [1] K. Nakamura *et al.* (Particle Data Group), *J. Phys.* **G37**, 075021 (2010).
- [2] Throughout this paper, all decay modes represent that mode and its charge conjugate.
- [3] D. J. Lange, *Nucl. Instrum. Methods Methods Phys. Res., Sect. A* **462**, 152 (2001).
- [4] S. Agostinelli *et al.* (GEANT4 Collaboration), *Nucl. Instrum. Methods Phys. Res., Sect. A* **506**, 250 (2003).
- [5] B. Aubert *et al.* (*BABAR* Collaboration), *Nucl. Instrum. Methods Phys. Res., Sect. A* **479**, 1 (2002).
- [6] B. Aubert *et al.* (*BABAR* Collaboration), *Phys. Rev. Lett.* **99**, 021603 (2007).
- [7] B. Aubert *et al.* (*BABAR* Collaboration), *Phys. Rev. D* **80**, 051105 (2009).